

Precise and Fast LIDAR via Electrical Asynchronous Sampling Based on a Single Femtosecond Laser

LIZONG DONG, QINGGAI MI, SIYU ZHOU, AND GUANHAO WU*

State Key Laboratory of Precision Measurement Technology and Instruments, Department of Precision Instrument, Tsinghua University, Beijing 100084, China

**guanhaowu@mail.tsinghua.edu.cn*

Abstract: LiDAR, using a laser-based ranging method for precise environmental 3D sensing, has numerous scientific and industrial applications. However, the challenge lies in simultaneously enhancing precision and update rate, hinders its application in more unexpected scenarios. To this end, an optical frequency comb with a stable repetition frequency and femtosecond pulse width was used as an advanced laser source. The LiDAR performance significantly improved in the micrometer and megahertz regimes using an asynchronous sampling ranging method of electrical pulses based on a single femtosecond laser. This overcame the limitation of traditional optical sampling approaches, achieving a 38.8 μm Allan deviation at an update rate of 1 MHz and 8.06 μm after 2 ms time-averaging. The proposed method used a single laser for fast metrology monitoring, 1 megapixel/s 3D imaging at the meter-level non-ambiguous range and contactless vital sign detection at the hundred-micrometer scale.

1. Introduction

Light detection and ranging (LiDAR) is crucial in the intelligent perception of autonomous vehicles and robots [1–4]. Intelligent driving systems must respond timely and precisely when confronted with unforeseen events, such as the presence of children or unknown obstacles. Conventional LiDAR requires measurement intervals of several hundred milliseconds and fails to provide timely protection for vulnerable lives in such situations. Precise and fast LiDAR detection allows decision-making for additional time, render it applicable in unexpected application as well [5–7]. For instance, in advanced manufacturing, it can be employed to monitor the conditions of aircraft turbine blades during high-speed rotation. In intelligent healthcare, high-resolution non-contact vital sign detection using LiDAR, such as the simultaneous monitoring of human movement, breathing, and heartbeat information, exceeds imagination.

LiDAR relies on the following two ranging technological approaches: time-of-flight (TOF) and frequency-modulated continuous-wave (FMCW) methods [8–11]. The precision and speed of conventional TOF are usually in the centimeter and kilohertz regimes, respectively, and limited by the light source performance and bandwidth of the electrical device [3]. In the FMCW method, the speed, range resolution, and accuracy depend on the stringent conditions of the frequency, agility, and linearity of the lasers. Additionally, complex signal processing at the backend leads to a trade-off between real-time, faster speed, and higher precision, posing a significant challenge to swept-frequency light sources [10, 11].

Recently, numerous studies have focused on utilizing femtosecond lasers as light sources to achieve rapid and high precision [12–15]. Dual-comb ranging (DCR) is one of the most effective methods. The fiber DCR method employs asynchronous optical sampling and exhibits outstanding performance, including micrometer-level precision and meter-level unambiguous range (NAR). Most DCR systems measure distances using the Fourier transform method (FFT). The Fourier spectrum of an interferogram comprises multiple longitudinal modes in the radio frequency domain. After low-pass filtering, the Fourier spectra ranges from 0 to $f_r/2$ (f_r

represents the repetition rate of the lasers). To obtain effective phase information, the frequency range of the spectra must not overlap with 0 or $f_i/2$ to prevent spectral aliasing, which disables the FFT [16]. To avoid the spectral aliasing problem, the update rate of the fiber dual comb is limited to the kilohertz range owing to its lower repetition frequency. To overcome this speed constraint, electro-optic (EO) combs and microcombs have been developed to achieve ultrahigh repetition rates that increase the update rate to the megahertz level [17–19]. However, owing to the large repetition rate of EO combs or microcombs, the NAR is very small and proportional to the inverse of the repetition rate, thus restricting their application to larger-range measurements [20–25].

Real-time processing is crucial for rapid metrology applications. Direct TOF detection enables a high update rate based on high-repetition-rate laser pulses. However, it requires high-bandwidth detectors and a high-sampling-rate acquisition device to satisfy the more precise requirements. To accurately obtain the time delay of pulses, a sufficient number of sampling points are required for waveform reconstruction involving an ultrahigh-sampling-rate device. In most DCR research, the distance is computed using the FFT algorithm, which relies on substantial data and requires sufficient time for complex computation [15, 16]. Consequently, using a high-sampling-rate device increases the workload for the acquisition system and algorithms. However, the increasing sampling rate restricts the storage depth and is limited by the speed of the analog-to-digital converter (ADC), cost, and associated large data processing requirements, necessitating the division of the acquisition and computation steps. These factors pose a significant challenge toward achieving real-time systems [20, 24].

This study proposes a simple and powerful TOF measurement method with asynchronous sampling of electrical pulses, overcoming the challenges posed by excessively high sampling rates and the tradeoff between precision and speed. This method enables high precision and fast update rate while maintaining a large NAR, thereby surpassing the limitations of state-of-the-art dual-comb optical asynchronous sampling methods. It also facilitates real-time computation and data output on integrated devices. Furthermore, the proposed method can dynamically tune the update rate without adjusting the optical cavity lengths of the lasers. In contrast to the conventional applications of frequency combs, we demonstrated several novel applications of the proposed LiDAR, including noncontact vital-sign detection, fast metrology real-time monitoring, and 3D imaging, with excellent performance.

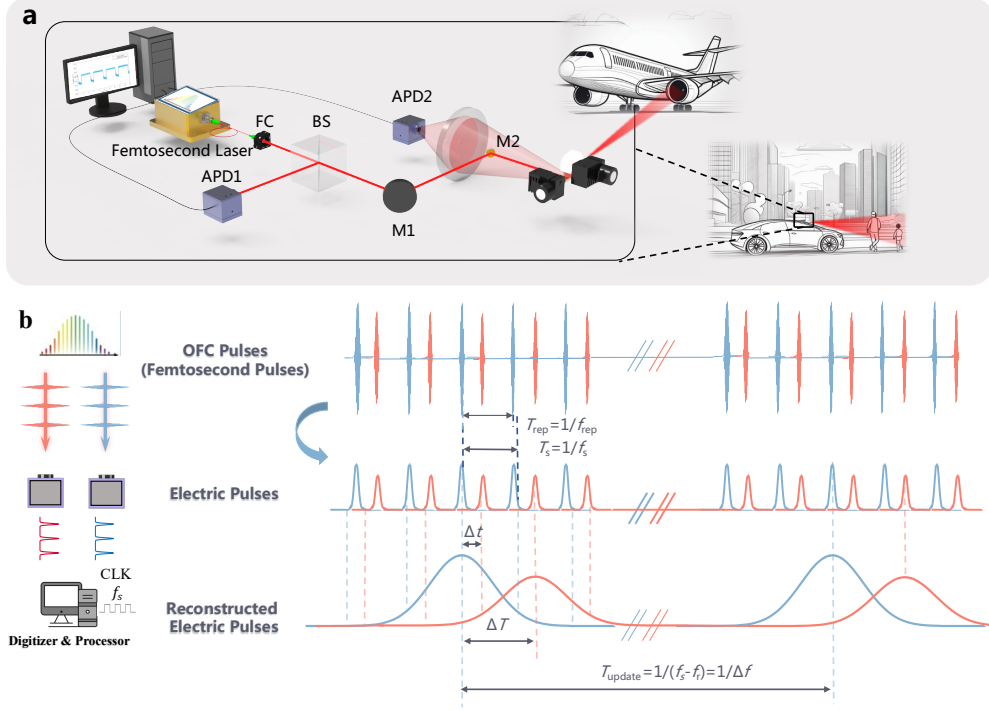


Fig. 1. Schematic and principle of the electrical asynchronous sampling ranging method. (a) Schematic of the optical system. BS: beam splitter; FC: fiber collimator; APD1-2: avalanche photodiode; M1-2: mirror; Femtosecond lasers with $f_{rep}=56.091$ MHz. (b) Principle of the asynchronous sampling method. A pair of repetition-rate-locked femtosecond laser trains are detected and photoelectrically converted using APD, forming a pair broadened electrical pulse trains. The waveforms are further broadened in time domain by asynchronous sampling under the sampling clock f_s . CLK: clock with $f_s = f_{rep} + \Delta f$ sine waveform. Optical pulses are converted to electrical pulses and high-repetition-frequency electrical pulses are reconstructed. Blue and orange pulses represent the reference and measurement signals, respectively. T_{rep} and T_s denote the periods of pulses and sampling, respectively.

2. Principle and precision analysis

2.1 Experimental setup and asynchronous sampling ranging method for electrical pulses

The proposed approach is based on a coaxial optical path, as shown in Fig. 1(a). It indirectly measures the TOF of the optical pulses by comparing the time delay between two periodic electrical waveforms from separate avalanche photodiodes (APD). The measurements were obtained from the two distinct pulse trains using a homemade Er-doped fiber femtosecond laser ($f_{rep} = 56.091$ MHz) divided by a 90:10 beam splitter. The pulse train serving as the reference beam was directed to one InGaAs APD for converting the optical pulses into electrical pulses. The other pulse train, serving as the target beam, was incident on the target. The returning pulse was focused on another APD through the emission and receiving coaxial optical paths. Two electrical pulse trains were recorded using a homemade 16-bit digitizer that could accept an external sampling clock, enabling simultaneous real-time recording on the two channels. The reference and measured electrical pulse signals were simultaneously digitized and recorded under a stable clock-sampling signal f_s , as shown in Fig. 1(b). Subsequently, the distance measurements were processed by combining the pulse location algorithm and system parameters. A Galvo scanner was applied to the coaxial optical path to realize 3D imaging, and the triggers for the Galvo scanning driver and data collection were set synchronously. The

measured distance (along with the scanning angle readings) was converted into Cartesian coordinates, resulting in a 3D point cloud.

To process two high-repetition-rate electrical waveforms, we proposed an asynchronous sampling ranging method for electrical pulses. We employed a sampling rate ($f_s = f_{\text{rep}} + \Delta f$) to the digitizer supplied by a frequency synthesizer. At the set clock rate, a single data point was captured per electrical pulse cycle. Subsequently, the next data point with a minute pulse shift was captured when the next clock cycle arrived. This process was iteratively performed before amplifying the waveforms and original time delays (Δt) of the target and reference beams, as depicted in Fig. 1(c). The two pulse trains were amplified by a factor of $f_{\text{rep}}/\Delta f$ in time domain to yield a pair of reconstructed pulses under a measured period ($T_{\text{update}}=1/\Delta f$), which represents the measurement acquisition rate. The relative amplified time delay (ΔT) was obtained by calculating the centroid between the amplified reference and target pulses. Subsequently, combined with the amplification coefficient, light speed, and refractive index of air, the absolute distance of the target was derived as

$$L = \frac{v_g}{2} \cdot \Delta T \cdot \frac{\Delta f}{f_{\text{rep}}} = \frac{v_g}{2} \cdot \Delta t \quad (1)$$

where L is the distance between the reference target and object, v_g is the group velocity of the femtosecond laser in air, ΔT is the amplified time-delay, and t is the original time delay. The electrical signals of the high-repetition-frequency femtosecond pulses were reconstructed using an asynchronous sampling ranging method that surpassed the bandwidth limitations of conventional devices.

The principle for achieving micrometer-level precision measurements is the amplification of the original minute-time delay through asynchronous sampling, which allows timing on a larger time scale. The upper limit of precision is influenced by the repetition rate difference (Δf), intensity noise of laser pulses, and the pulse localization algorithm (see Supplementary Information for details). The asynchronous sampling method can be further extended to the periodic multi-sampling method with a faster update rate and periodic under-sampling method with a lower requirement for the acquisition component (see Supplementary Information). The acquisition rate and precision can be switched by adjusting the sampling clock rate and selecting a matching algorithm without laser tuning. The following experimental data with slightly different setting update rates were obtained using this method.

2.2 Precision analysis

To evaluate the precision of the proposed asynchronous sampling ranging method, the distance from a fixed noncooperative target was measured at an update rate of 1 MHz using the extended multisampling method. Figure 2(a) shows the measurement of 5 ms, including the original data (blue point) and Kalman filtered data (red point). The Allan deviation, which was used to assess the repeatability of the proposed method, was analyzed for the 5 s data point, as shown in Fig. 2(b). The precision of the original data was 406.8 μm without time-averaging and it decreased to 8.06 μm with an averaging of 2 ms. To further suppress the noise in the original data while maintaining the measurement speed, the Karman filter (KF) was applied to improve the precision to 38.8 μm at an update rate of 1 MHz (see Supplementary Information for KF) [26]. For distance measurement, the accuracy of the proposed system was assessed via comparative experiments using a commercial laser interferometer (PT-313B) with an accuracy of 1 nm. A moving target corner mirror positioned at ~ 1 m was measured at a discrete moving step of 1 cm and range of 20 cm on the guide rail. Figures 2(c) and (d) shows the measurement accuracy result of the proposed system. Both ranging results were calculated under identical environmental parameters, including temperature, humidity, and air pressure, inducing an uncertainty of $\sim 10^{-7}$. By applying linear fitting [Fig. 2(c)], the slope and correlation coefficient (R^2) were obtained as 1.00078223 and 0.999999925, respectively. The residuals were within

$\pm 50 \mu\text{m}$ with a standard deviation of $23.74 \mu\text{m}$ [Fig. 2(d)] owing to the electrical noise of the detector.

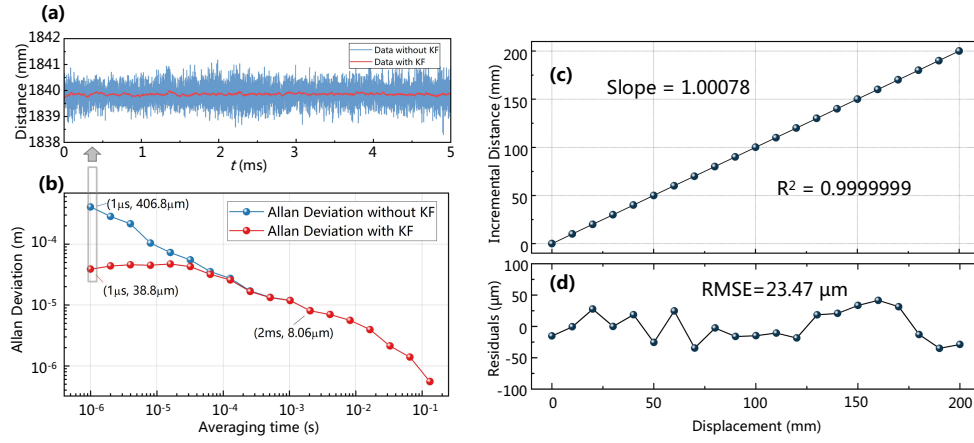


Fig. 2. Precision analysis. (a) Results of 1 MHz TOF measurements in within an acquisition time of 5 ms when the system update rate was set to 1 MHz. (b) Allan deviation of the distance measurement versus averaging time evaluated over the 5 s data point. Blue and red lines represent the original measurement result without filter and with the Kalman filter, respectively. After averaging for 2 ms, the precision of the two measurements decreased to $8.06 \mu\text{m}$. (c) Experimental evaluation of the measurement accuracy compared with that obtained using a commercial laser interferometer. Comparison of incremental distance measured by the proposed ranging system (vertical axis) with the displacements measured by a commercial laser interferometer (horizontal axis) at a distance of $\sim 1 \text{ m}$ with a moving step of $\sim 10 \text{ mm}$. (d) Residuals within $\pm 50 \mu\text{m}$.

3. Results

3.1 Verification of fast metrology monitoring

Turbines have become indispensable components of the modern aircraft. The state of turbine blades at different rotational speeds and vibration modes significantly affects the overall engine performance. Turbines often operate at speed exceeding ten thousand revolutions per minute (RPM); however, the existing laser measurement methods have not yet met the demands of real-time fast metrology monitoring (see the application scene in Fig. 3(a)). The proposed measurement method offers a novel solution for monitoring the rotating states of turbines.

The profile of a rapidly rotating fan was measured to validate the reproducibility and capability of the proposed system for rapid metrology. In this experiment, the measurement beam was focused on the surface of the fan blade, which rotated at a speed exceeding 10000 RPM, as shown in Fig. 3(a). The image shows the rotating direction of the fan and fixed detection position of the laser measurement. The distance-acquisition rate was set to 500 kHz. The dynamic measurement results, including the data for the fan blade and fixed clamping element, were reconstructed as shown in Fig. 3(b). The Kalman filter results (black line) were used to eliminate the noise by sacrificing a short transition time. At a rotation speed of 6000 RPM, the fan blade profile was simultaneously captured and reconstructed using over 300 data points. Owing to the insufficient dynamic balance characteristics of the fan, the high-speed rotation at a fan rotation speed of 10000 RPM caused vibrations in a specific range affecting the supporting device. Figure 3(c) shows a sinusoidal resonance background movement with an amplitude of 2 mm, precisely matching the rotation rate of 166.6 Hz.

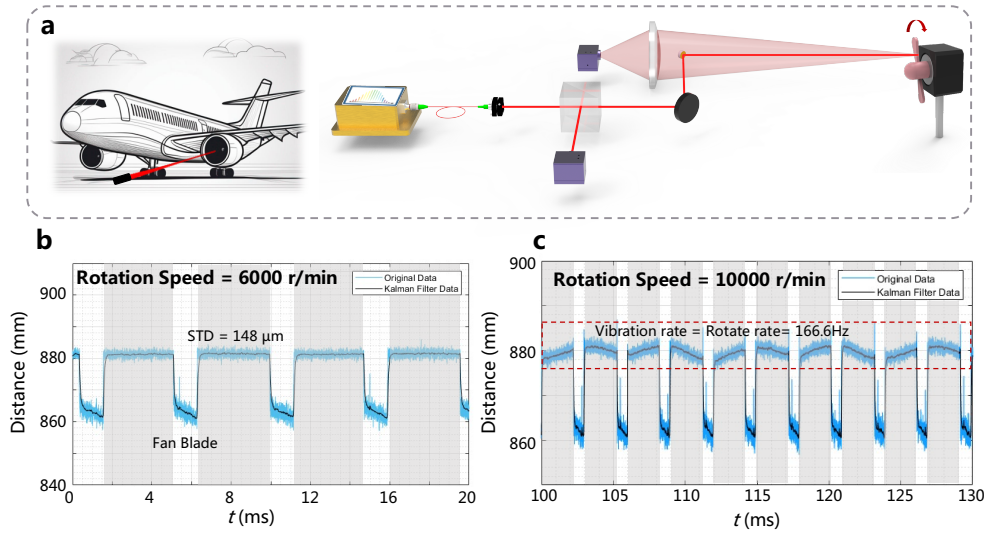


Fig. 3. Results of fast metrology with a highly rotating object. (a) Application to turbine monitoring and measurement for high-rotation-speed fan. The laser light is emitted by the previously mentioned experimental setup toward the fan blade and background. The record data includes the distance and other status information. (b) Measurement result under 6000 rpm. The standard deviation of the background is approximately 148 μm . (c) Measurement result of 10000 rpm. The vibration rate of background is equal to the rotation rate.

3.2 3D imaging

This section demonstrates the ability of the proposed ranging system to achieve submillimeter-level resolution and meter-level NAR 3D imaging. The applied clock rate was $f_s = 113.182$ MHz and acquisition rate was 1 MHz, i.e., the 3D imaging system attained a point rate of 1 MP/s using a single laser. A scene containing a model gate of Tsinghua University, two model cars, and “THU” characters with a distance spacing in the range 5–10 cm were created and positioned at a distance of ~ 1 m in front of the scanning mirror [see Fig. 4(a)]. Figure 4(b) shows the front and top views of the reconstructed scene 3D image with a resolution of 180000 pixels (600 L, 300 H, each point was calculated as the average of 50 ranging results). A portion of the detailed point cloud was represented by characters “THU” [see Fig. 4(d)]. The protrusions on “THU” are the joints of the building blocks. According to the product manual, each joint had a radius of 4.8 mm and height of 1.7 mm. Figure 4(e) shows the details of the joint point cloud. The excellent vertical and horizontal range resolutions of the imaging system facilitate the clear visualization of sub-millimeter-level details at the meter-level scale.

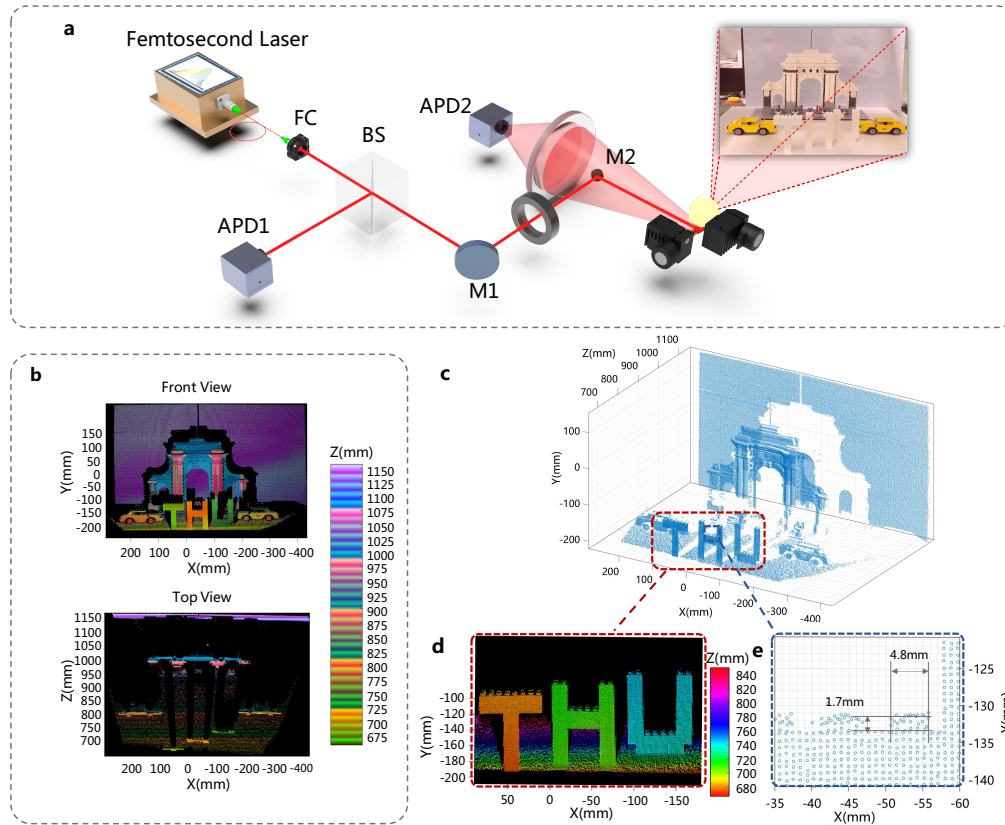


Fig. 4. 3D scanning imaging. (a) Experimental setup. Laser beam is steered by the galvanometer scanner. The constructed scene includes various types of plastic models. (b) Front and top views of the point cloud with linear striped pseudo colored rendering. (c) 3D image reconstructed by the combination of distance measurement and angle-record. (d) Details of the “THU” characters. (e) Details of the protrusions, which are the joints in the building blocks. Each protrusion has a radius and height of 4.8 and 1.7 mm, respectively.

3.3 Noncontact vital sign monitoring

To further validate the excellent distance resolution and universality of the proposed LiDAR system, an experiment was performed to assess the vital signs of the human body, including breath and heartbeat information. Vital sign detection is widely implemented in medical and health settings using contact and wearable sensors. However, they are unsuitable for patients with burn wounds or other skin conditions, necessitating the requirement of noncontact detection. Figure 5(a) shows the experimental setup involving femtosecond lasers directed at the chest of the testing personnel. This approach allowed the observation of variations in chest contours caused by breathing and heartbeat movements, thereby enabling the measurement of breathing rate, heart rate, and other physiological parameters. Typically, the respiratory movement can cause micro-motions in the chest wall of approximately 1 to 12 mm, whereas the cardiac movement can generate micro-motions of approximately 100 to 500 μm . The heartbeat of healthy adults typically falls in the range 0.8–2 Hz, whereas the breathing rate is in the range 0.1–0.5 Hz. These two signals can be extracted and identified separately using different bandpass filters.

Figure 5(b) shows the chest motion information obtained from the measurements on the testing personnel while sitting. The respiratory rate is approximately 0.34 Hz (20.4 breaths per min) and the distance variation caused by the motion is approximately 5 mm. After removing the motion artifacts and extracting them using a bandpass filter, the heartbeat-induced chest

contour fluctuations were obtained. These fluctuations exhibited an amplitude of approximately $300\ \mu\text{m}$ at a frequency of $1.54\ \text{Hz}$ (92.4 heartbeats per min), as indicated by the red line. The time–frequency graph was obtained by calculating the data in Fig. 5(b) using a short-time FFT. Three purple peaks were observed at all times, with frequencies increasing in the following order: respiratory signal, second harmonic of the respiratory signal, and heartbeat signal. The time–frequency graph obtained by performing a short-time FFT with the normalized amplitude was plotted, yielding a breathing rate and heart rate of $20.4/\text{min}$ and $92.4/\text{min}$, respectively, as shown in Fig. 5(c). Two vibration rates can be observed in the spectrum obtained from the Fourier transform of the total signal, with the amplitude of the respiratory motion being approximately $22\ \text{dB}$ higher than that of the heartbeat motion. The high-range resolution of the proposed system enabled accurate respiratory detection during human breathing.

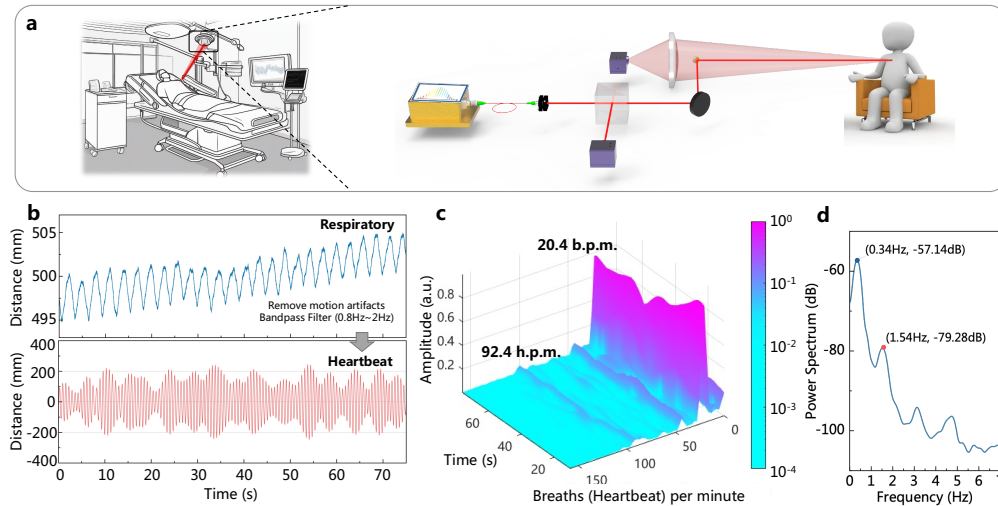


Fig. 5. Results of single-point measurement for vital signs monitoring. (a) Schematic application of vital sign measurement and experimental setup. The laser is emitted by the proposed experimental setup and directed toward the chest area for monitoring. (b) Results of overall signs, including breaths and heartbeat movements with an amplitude of $5\ \text{mm}$ shown as the blue line. Results of heart movement shown as the red line. The heartbeat signal is obtained after specific filtering (bandwidth $0.8\text{--}2\ \text{Hz}$), shown as the red line data with an amplitude of approximately $300\ \mu\text{m}$. (c) Time–frequency graph obtained by performing the short-time FFT on the data in (b) with a normalized amplitude normalized. The breathing and heart rates are 20.4 and 92.4 per minute, respectively. (d) Power spectrum shows that the respiratory rate is $0.34\ \text{Hz}$ and heartbeat rate is approximately $1.54\ \text{Hz}$. The amplitude of breaths is $22\ \text{dB}$ higher than that of heartbeats.

4. Discussion and conclusion

This study achieved high-precision and fast-speed femtosecond LiDAR based on asynchronous sampling of electrical pulses, yielding a precision of $38.8\ \mu\text{m}$ at an update rate of $1\ \text{MHz}$ and $8.06\ \mu\text{m}$ after time-averaging of $2\ \text{ms}$. This overcomes the limitations of measurement speed and ranging precision of the conventional TOF LiDAR systems. Compared to state-of-the-art dual-comb methods, the proposed method surpasses the Nyquist sampling limit of interferometric optical asynchronous sampling and boasts ultrafast real-time measurements and data output.

Experiments verified the outstanding performance of the proposed method in the fast metrology of profiles and vibrations, high-range resolution 3D imaging, and real-time detection of human vital signs. The method balanced the measurement speed, precision, and range and enhanced LiDAR for unexpected scenarios.

The proposed femtosecond LiDAR system can achieve a faster measurement speed by enhancing the repetition rate of the femtosecond laser and detectors with a wider bandwidth,

including the use of an EO comb or micro-comb with a repetition frequency of up to GHz [17, 27]. Higher precision, longer range, and small-volume integration of products could be achieved by transforming the spatial optical system structure into a fiber optical path, applying an Er-doped optical fiber amplifier in the receiver optical path, and changing the APD to a single-photon detector. Furthermore, low-cost compact fiber lasers and prospective on-chip femtosecond lasers can potentially reduce the cost of the LiDAR system, paving the way for intelligent application scenarios.

Funding

National Natural Science Foundation of China (Grants No. 62227822, 52105555, 92150104)

Acknowledgments

We thank Prof. Yang Li and Prof. Yuanmu Yang for their helpful suggestions and discussion. We thank Hao Ouyang and Xingyu Jia for their help with figures and experiments.

Disclosures

The authors declare no conflicts of interest.

Data availability

Data underlying the results presented in this paper are not publicly available at this time but may be obtained from the authors upon reasonable request.

Supplemental document

See Supplement 1 for supporting content.

References

1. Schwarz B. Mapping the world in 3D[J]. *Nature Photonics*, 2010, 4(7): 429-430.
2. S. Royo and M. Ballesta-Garcia, "An overview of lidar imaging systems for autonomous vehicles," *Appl. Sci.* **9**(19), 4093 (2019).
3. B. Behroozpour, P. A. M. Sandborn, M. C. Wu, B. E. Boser, "Lidar system architectures and circuits," *IEEE Commun. Mag.* **55**(10), 135-142 (2017).
4. R. Roriz, J. Cabral, and T. Gomes, "Automotive LiDAR technology: A survey," *IEEE Trans. Intell. Transp. Syst.* **23**(7), 6282-6297 (2021).
5. Z. Zhang, Y. Liu, T. Stephens, B. J. Eggleton, "Photonic radar for contactless vital sign detection," *Nat. Photon.* **17**(9), 791-797 (2023).
6. L. Dong, Q. Mi, S. Zhou, et al., "High-Speed and High-Precision Ranging System for Non-Cooperative Targets based on Optical Frequency Comb," *CLEO: Applications and Technology. Optica Publishing Group*, (2023), Vol. 7, p. ATh1K.
7. Teleanu E L, Durán V. Electro-optic dual-comb interferometer for high-speed vibrometry[J]. *Optics Express*, 2017, 25(14): 16427-16436.
8. N. Kuse and M. E. Fermann, "Frequency-modulated comb LIDAR," *Apl. Photonics* **4**(10) (2019).
9. Lukashchuk A, Riemensberger J, Karpov M, et al. Dual chirped microcomb based parallel ranging at megapixel-line rates[J]. *Nature Communications*, 2022, 13(1): 3280.
10. Roos P A, Reibel R R, Berg T, et al. Ultrabroadband optical chirp linearization for precision metrology applications[J]. *Opt. letters*, 2009, 34(23): 3692-3694.
11. Komissarov R, Kozlov V, Filonov D, et al. Partially coherent radar unites range resolution from bandwidth limitations[J]. *Nature communications*, 2019, 10(1): 1423.
12. I. Coddington, W. C. Swann, L. Nenadovic, N. R. Newbury, "Rapid and precise absolute distance measurements at long range," *Nat. Photonics* **3**(6), 351-356 (2009).
13. J. Lee, Y. J. Kim, K. Lee, S. Lee, S. Kim, "Time-of-flight measurement with femtosecond light pulses," *Nat. Photonics* **4**(10), 716-720 (2010).
14. Wang J, Lu Z, Wang W, et al. Long-distance ranging with high precision using a soliton microcomb[J]. *Photonics Research*, 2020, 8(12): 1964-1972.
15. Z. Zhu and G. Wu, "Dual-comb ranging," *Engineering* **4**(6), 772-778 (2018).
16. R. Jiang, S. Zhou, and G. Wu, "Aliasing-free dual-comb ranging system based on free-running fiber lasers," *Opt. Express* **29**(21), 33527-33535 (2021).
17. R. Zhuang, K. Ni, G. Wu, T. Hao, L. Lu, Y. Li, Q. Zhou, "Electro-optic frequency combs: Theory, characteristics, and applications," *Laser Photonics Rev.* **17**(6), 2200353 (2023).

18. M. Zhang, B. Buscaino, C. Wang, A. Shams-Ansari, C. Reimer, R. Zhu, J. M. Kahn, M. Lončar, "Broadband electro-optic frequency comb generation in a lithium niobate microring resonator," *Nature* **568**(7752), 373-377 (2019).
19. M. G. Suh and K. J. Vahala, "Soliton microcomb range measurement," *Science* **359**(6378), 884-887 (2018).
20. Y. Na, C. G. Jeon, C. Ahn, M. Hyun, D. Kwon, J. Shin, J. Kim, "Ultrafast, sub-nanometre-precision and multifunctional time-of-flight detection," *Nat. Photonics* **14**(6), 355-360 (2020).
21. X. Zhang, K. Kwon, J. Henriksson, J. Luo, M. C. Wu, "A large-scale microelectromechanical-systems-based silicon photonics LiDAR," *Nature* **603**(7900), 253-258 (2022).
22. R. Chen, H. Shu, B. Shen, L. Chang, W. Xie, W. Liao, Z. Tao, J. E. Bowers, X. Wang, "Breaking the temporal and frequency congestion of LiDAR by parallel chaos," *Nat. Photon.* **17**(4), 306-314 (2023).
23. J. Riemensberger, A. Lukashchuk, M. Karpov, W. Weng, E. Lucas, J. Liu, T. J. Kippenberg, "Massively parallel coherent laser ranging using a soliton microcomb," *Nature* **581**(7807), 164-170 (2020).
24. P. Trocha, M. Karpov, D. Ganin, M. H. P. Pfeiffer, A. Kordts, S. Wolf, J. Krockenberger, P. Marin-Palomo, C. Weimann, S. Randel, W. Freude, T. J. Kippenberg, C. Koos, "Ultrafast optical ranging using microresonator soliton frequency combs," *Science* **359**(6378), 887-891 (2018).
25. Bao C, Suh M G, Vahala K. Microresonator soliton dual-comb imaging[J]. *Optica*, 2019, 6(9): 1110-1116.
26. D. Hu, Z. Wu, H. Cao, Y. Shi, R. Li, H. Tian, Y. Song, M. Hu, "Dual-comb absolute distance measurement of non-cooperative targets with a single free-running mode-locked fiber laser," *Opt. Commun.* **482**, 126566 (2021).
27. Snigirev V, Riedhauser A, Lihachev G, et al. Ultrafast tunable lasers using lithium niobate integrated photonics[J]. *Nature*, 2023, 615(7952): 411-417.